Electronic Supplementary Material (ESI) for Materials Advances.

Engineering manganese-based oxide heterostructure cathode for high-performance aqueous potassium-ion storage

Zheng Guan[a], Yunan Wang[a], Mingyue Zhang[a], Jie Liu[b], Shuangwen Li[c], Di Guo[a,*], Xiaoxia Liu [a,*]

[a]Department of Chemistry, Northeastern University, Shenyang, 110819, China

[b]School of Resources and Civil Engineering, Northeastern University, Shenyang, 110819, China

[c]School of Materials Engineering, North China Institute of Aerospace Engineering, Langfang, 065000, China

*Corresponding author: Di Guo, guodi@mail.neu.edu.cn

Xiaoxia Liu, xxliu@mail.neu.edu.cn

1. Computational formula

Specific capacity of different samples according to the constant current charge-discharge profiles are calculated from equation 1 [1,2]:

$$C = \frac{It}{m} \qquad \text{(Eq. S1)}$$

where C stands for specific capacitance (mAh g^{-1}), I is the discharge current (mA), t is the discharge time (h), m is the mass loading of the active materials (g).

The log(i) versus log(ν) plot for the cathodic and anodic peak shows that the current dependence on the scan rate, ν, is given by the relation [3]:

$$i(V) = av^b \qquad \text{(Eq. S2)}$$

The current response at a fixed potential can be expressed as the combination of two separate mechanisms, surface capacitive effects and diffusion-controlled insertion processes [4]:

$$i(V) = k_1 v + k_2 v^{1/2} \qquad \text{(Eq. S3)}$$

$k_1\nu$ and $k_2\nu^{1/2}$ correspond to the current contributions from the surface capacitive effects and the diffusion-controlled intercalation process, respectively. Thus, by determining k_1 and k_2, we are able to quantify, at specific potentials, the fraction of the current due to each of these contributions.

2. Figures and tables

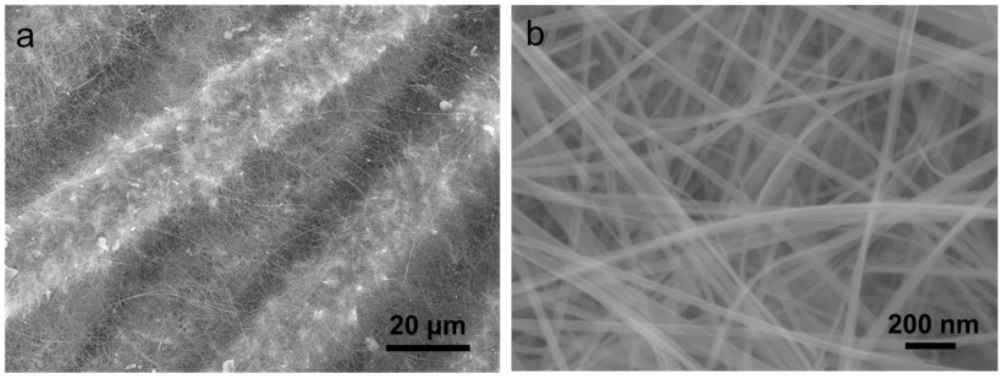

Fig. S1. SEM image of pure Mn_3O_4 at low magnification (a) and high magnification (b).

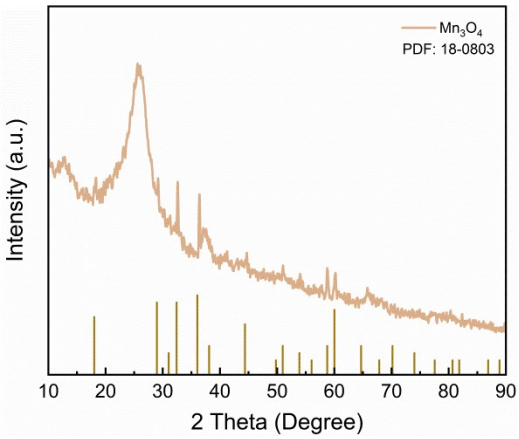

Fig. S2. The XRD spectra of pure Mn_3O_4.

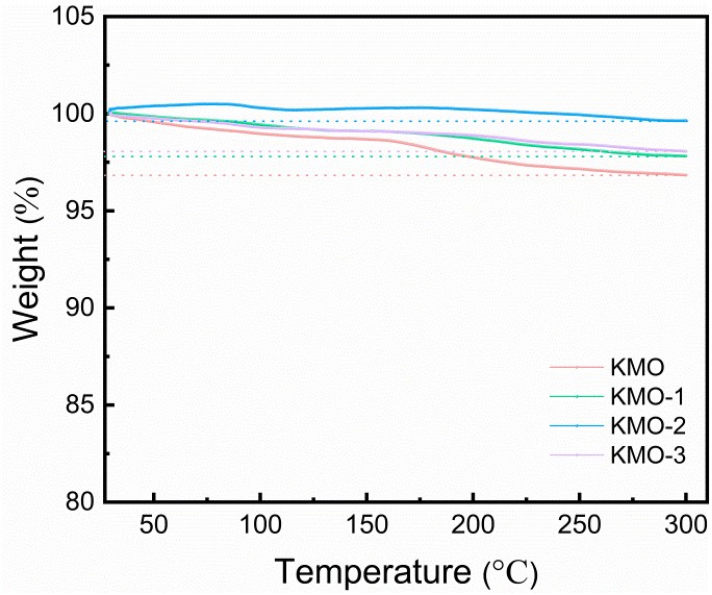

Fig. S3. TGA curves of KMO-KMO-3 from room temperature to 300 ℃ at a ramping rate of 3 ℃ min^{-1} under N_2 flow.

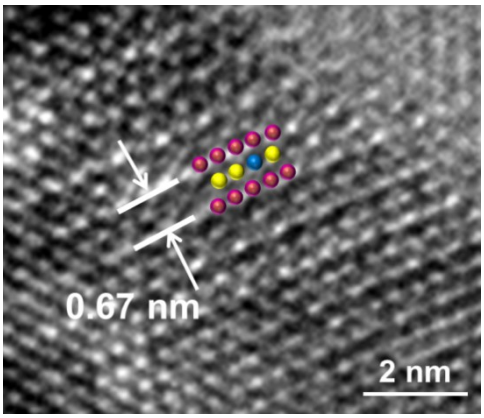

Fig. S4. Enlarged HRTEM image of the birnessite nanosheet in KMO-2.

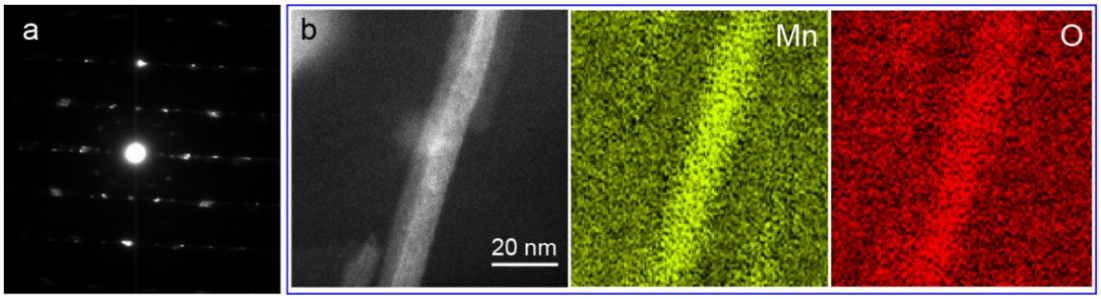

Fig. S5. (a) The SAED pattern for Mn_3O_4 nanowires in KMO-2. (b) STEM image of a Mn_3O_4 nanowire in KMO-2 with corresponding EDS elemental mappings of Mn and O.

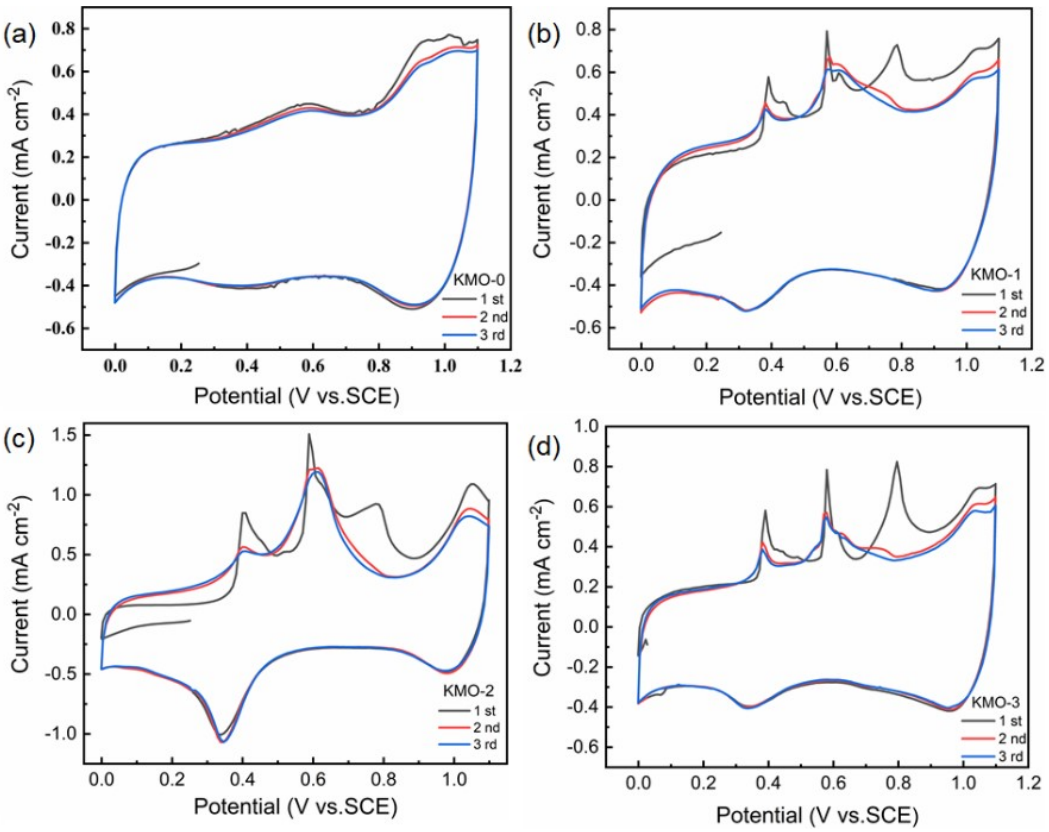

Fig. S6. The initial three CV curves of KMO-KMO-3 electrodes at a scan rate of 0.3 mV s^{-1}.

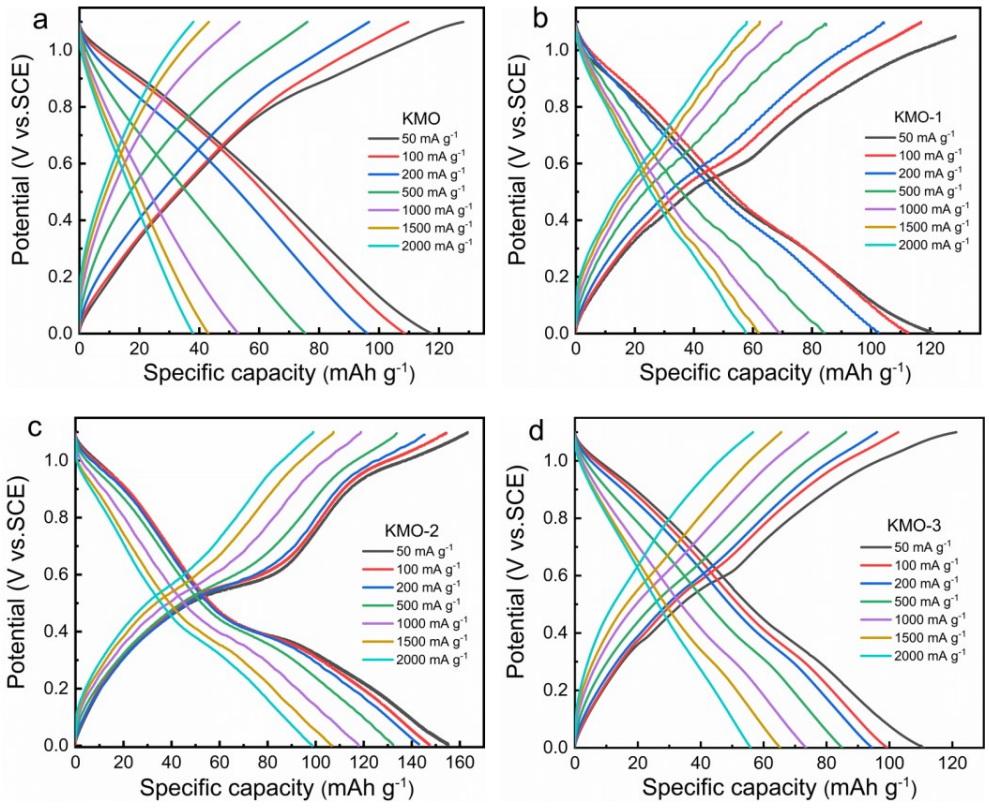

Fig. S7. Galvanostatic charge/discharge curves of the KMO-KMO-3 electrodes at various current densities of 50-2000 mA g^{-1}, respectively.

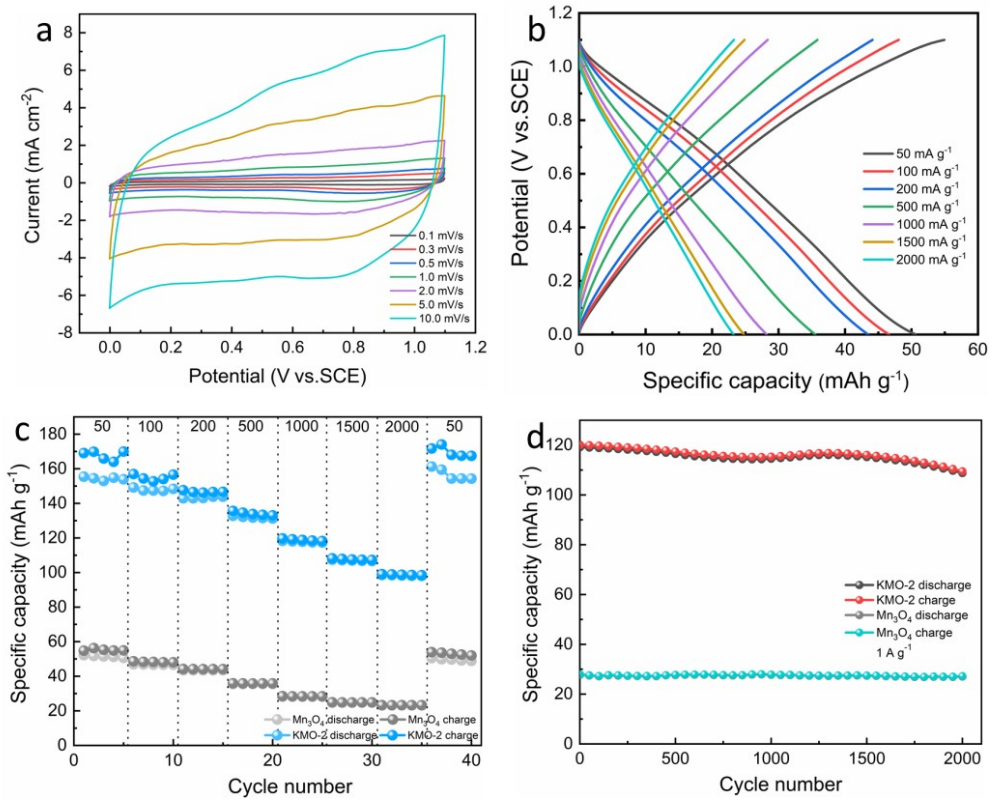

Fig. S8. (a) CV curves of pure Mn_3O_4 at the scan rates of 0.1-10 mV s^{-1}. (b) Galvanostatic charge/discharge profiles of pure Mn_3O_4 at the different current densities of 50-2000 mA g^{-1}. (c) Rate capability comparison of the KMO-2 and Mn_3O_4 electrode. (d) Cyclic stability comparison of the KMO-2 and Mn_3O_4 electrode.

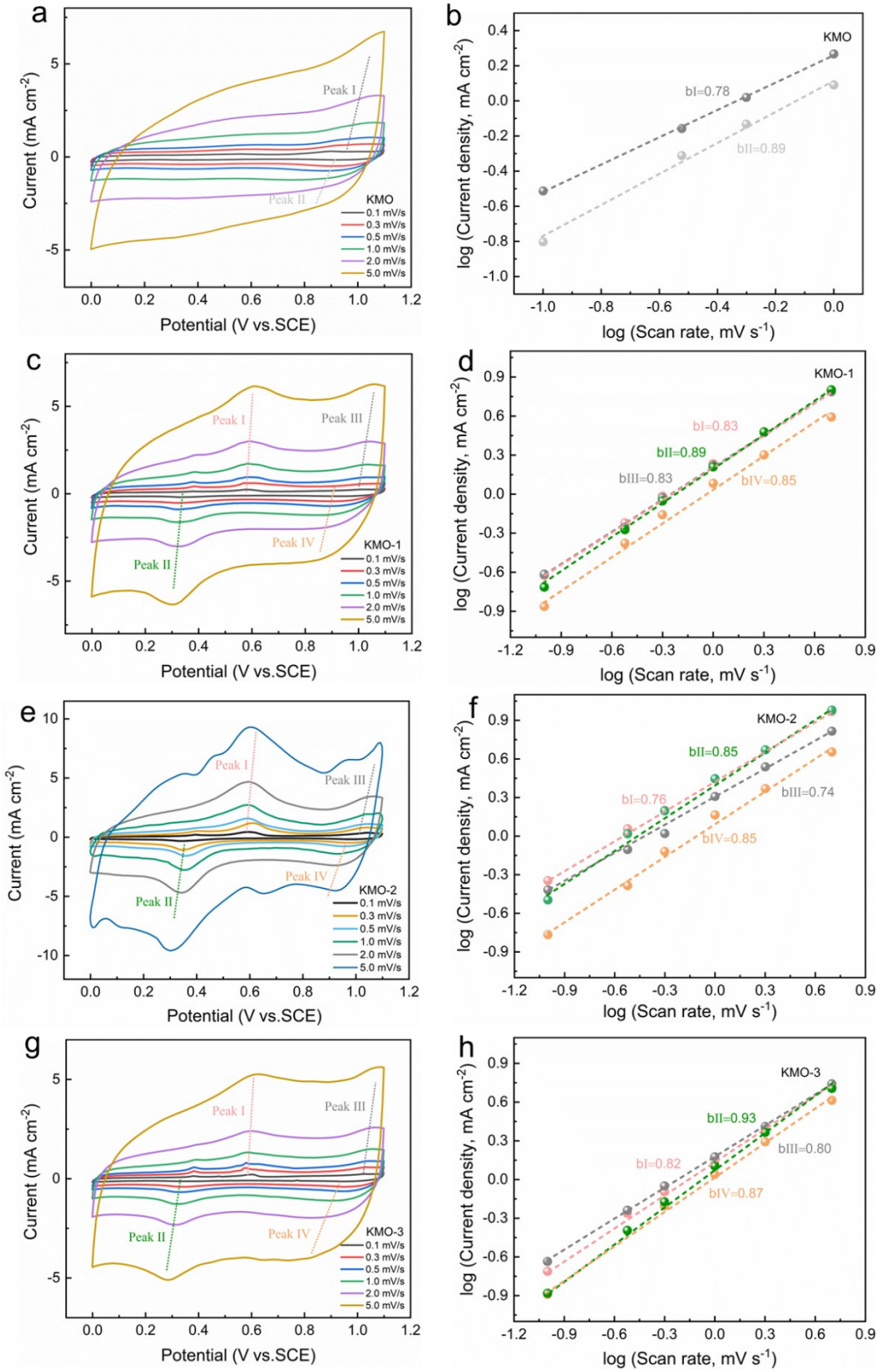

Fig. S9. CV curves of KMO (a), KMO-1 (c), KMO-2 (e) and KMO-3 (g) at the scan rates of 0.1-5 mV s^{-1} and the log(i) versus log(v) plot of the peak current response of KMO (b), KMO-1 (d), KMO-2 (f) and KMO-3 (h).

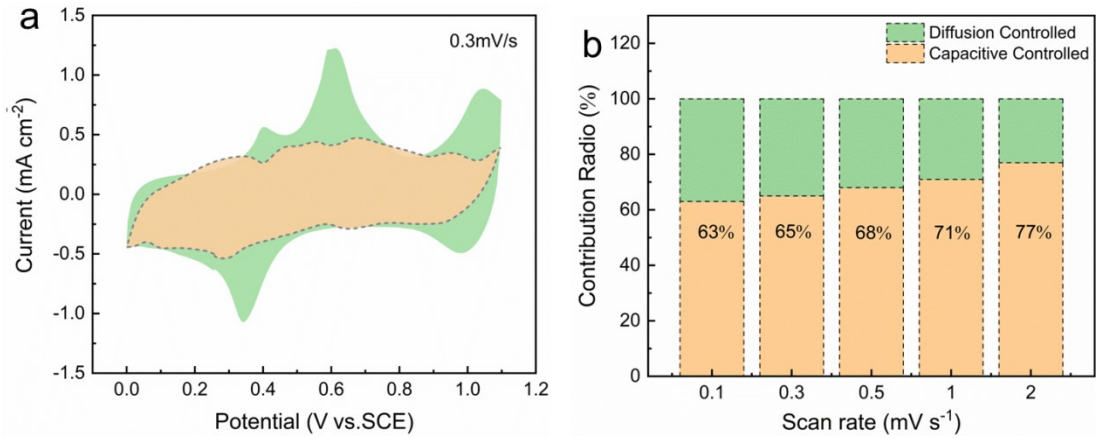

Fig. S10. (a) The capacitive-controlled (orange) and diffusion-controlled (green) contribution to the charge storage of KMO-2 at 0.3 mV s^{-1}. (b) Normalized contribution ratio of capacitive (orange) and diffusion-controlled (green) capacities of KMO-2 at different scan rates.

Table S1. The Mn^{2+}, Mn^{3+} and Mn^{4+} percentage of KMO, KMO-1, KMO-2 and KMO-3 sample determined by XPS.

electrode	**Mn^{4+}**	**Mn^{3+}**	**Mn^{2+}**	**Average valence**
KMO	69.5%	30.5%	0	3.695
KMO-1	44.1%	39.4%	16.5%	3.276
KMO-2	39.5%	42.2%	18.3%	3.212
KMO-3	33.1%	44.9%	22%	3.111

Table S2. The crystal water contents of KMO, KMO-1, KMO-2 and KMO-3 sample determined by TG.

electrode	**Crystal water contents**
KMO	3.16% wt.
KMO-1	2.18% wt.
KMO-2	0.36% wt.
KMO-3	1.94% wt.

Table S3. The ICP result of K/Mn ratio in KMO-KMO-3

electrode	**K/Mn Ratio**
KMO	0.15
KMO-1	0.17
KMO-2	0.21
KMO-3	0.18

Table S4. The molecular formula of KMO-KMO-3 determined by ICP, TG and XPS data.

electrode	Chemical formula
KMO	$K_{0.15}MnO_2 \cdot 0.97H_2O$
KMO-1	$K_{0.43}MnO_2 \cdot 1.49H_2O + Mn_3O_4$ (46.87%)
KMO-2	$K_{0.52}MnO_2 \cdot 0.22H_2O + Mn_3O_4$ (50.12%)
KMO-3	$K_{0.57}MnO_2 \cdot 1.64H_2O + Mn_3O_4$ (54.30%)

Table S5. Electrochemical performance comparison between previously reported high-stable cathodes and the KMO-2 cathode in the present work for APIBs

Electrode	Electrolyte	Potential window	Specific capacitance	Cyclic stability
$K_2Fe^{II}[Fe^{II}(CN)_6] \cdot 2H_2O$ [1]	0.5 M K_2SO_4	0-1.2 V (vs. Ag/AgCl)	120 mAh g^{-1} at 200 mA g^{-1}	86% (500 Cycles at 2A g^{-1})
PG ($Fe^{III}Fe^{III}(CN)_6$)[2]	1 M KNO_3	0-1.0 V (vs. Ag/AgCl)	123 mAh g^{-1} at 111 mA g^{-1}	44.7% (1100 Cycles at 500 mA g^{-1})
PG ($FeFe(CN)_6$)[3]	Saturated KNO_3	-0.2-1.1 V (vs. SCE)	120 mAh g^{-1} at 360 mA g^{-1}	90.5%(300 Cycles at 360 mA g^{-1})
$K_{1.93}Fe[Fe(CN)_6]_{0.97} \cdot 1.82H_2O$[4]	1 M KNO_3	-0.2-1.0 V (vs. SCE)	142 mAh g^{-1} at 75 mA g^{-1}	88% (300 Cycles at 1.5 A g^{-1})
$K_{1.82}Mn[Fe(CN)_6]_{0.96} \cdot 0.47H_2O$[5]	21M KCF_3SO_3	0-1.25V (vs. Ag/AgCl)	160 mAh g^{-1}at 300 mA g^{-1}	100% (130000 Cycles at 2.5 A g^{-1})
$K_{1.43}Co[Fe(CN)_6]_{0.94} \cdot 1.87H_2O$[6]	22M KCF_3SO_3	0-1.2 V (vs. Ag/AgCl)	90 mA h g^{-1} at 20 mA g^{-1}	70% (1000 Cycles at 600 mA g^{-1})
$K_2NiFe(CN)_6 \cdot 1.2H_2O$ [7]	1M KNO_3 per 0.01 M HNO_3	0-1.0 V (vs. SCE)	77.4 mAh g^{-1}at 400 mA g^{-1}	98.6% (5000 Cycles at 2.4 A g^{-1})
$K_xFe_yMn_{1-y}[Fe(CN)_6]_w \cdot zH_2O$[8]	22 M KCF_3SO_3	0-1.2 V (vs. Ag/AgCl)	135 mAh g^{-1} at 65 mA g^{-1}	90% (10000 Cycles at 13 A g^{-1})

$K_{0.22}V_{1.74}O_{4.37}$ ·0.82 H_2O[9]	1M KCl	-0.1-0.9 V (vs. Ag/AgCl)	183 mAh g^{-1} at 5 mV s^{-1}	nearly100% (5000 Cycles at 2-20 A g^{-1}, full-cell)
$K_{0.52}MnO_2$·0.22H_2O+ Mn_3O_4 (50.12%) (This work)	**Saturated K_2SO_4**	**0-1.1 V (vs. SCE)**	**147 mAh g^{-1} at 100 mA g^{-1}**	**91.7% (2000 Cycles at 1 A g^{-1})**

References

[1] D.W. Su, A. McDonagh, S.Z. Qiao, G.X. Wang, *Adv. Mater.*, 2017, **29**, 1604007.

[2] P. Padigi, J. Thiebes, M. Swan, G. Goncher, D. Evans, R. Solanki, *Electrochimi. Acta*, 2015, **166**, 32-39.

[3] M.T. Wang, H.Q. Wang, H.M. Zhang, X.F. Li, *J. Energy Chem.*, 2020, **48**, 14-20.

[4] C. Li, X. Wang, W. Deng, C. Liu, J. Chen, R. Li, M. Xue, *ChemElectroChem*, 2018, **5**, 3887-3892.

[5] J. Ge, L. Fan, A.M. Rao, J. Zhou, B. Lu, *Nat. Sustain.*, 2022, **5**, 225-234.

[6] K.J. Zhu, Z.P. Li, T. Jin, L.F. Jiao, *J. Mater. Chem. A*, 2020, **8**, 21103-21109.

[7] W. Ren, X. Chen, C. Zhao, *Adv. Energy Mater.*, 2018, **8**, 1801413.

[8] L. Jiang, Y. Lu, C. Zhao, L. Liu, J. Zhang, Q. Zhang, X. Shen, J. Zhao, X. Yu, H. Li, *Nat. Energy*, 2019, **4**, 495-503.

[9] D.S. Charles, M. Feygenson, K. Page, J. Neuefeind, W.Q. Xu, X.W. Teng, *Nat. Commun.*, 2017, **8**, 1-8.